Preparation and Characterization of Fe/TiO_2 Photocatalyst for Visible Light Deep Desulfurization

By

Cheng Yee Yin

14213

Dissertation submitted in partial fulfilment of

the requirements for the

Bachelor of Chemical Engineering (Hons)

May2014

Universiti Teknologi PETRONAS

Bandar Seri Iskandar

31750 Tronoh

Perak Darul Ridzuan

Certification of Approval

Preparation and Characterization of Fe/TiO_2 Photocatalyst for Visible Light Deep Desulfurization

by

Cheng Yee Yin

14213

A project dissertation submitted to the

Chemical Engineering Programme

Universiti Teknologi PETRONAS

in partial fulfilment of the requirement for the

BACHELOR OF ENGINEERING (Hons)

(CHEMICAL ENGINEERING)

Approved by,

_____

(PROF T. MURUGESAN)

UNIVERSITI TEKNOLOGI PETRONAS

TRONOH, PERAK

SEPT 2014

Certification of Originality

This is to certify that I am responsible for the work submitted in this project, that the original work is my own except as specified in the references and acknowledgements, and that the original work contained herein have not been undertaken or done by unspecified sources or persons.

_____

(CHENG YEE YIN)

Abstract

With the high concern related to sulfur content in diesel oil, Malaysia is working towards reducing the sulfur content in diesel from 300 ppm to 10 ppm. The primary objective of this work is to prepare and characterize Fe/TiO_2 for visible light deep desulfurization. Titanium dioxide photocatalysis is the most effective photooxidative extractive sulfur removal. With the help of metal doping, the performance of desulfurization can be improved. Thus, loading of Fe onTiO_2 is used in this experiment to investigate the performance of desulfurization under visible light. A wet impregnation method is used to prepare Fe/TiO_2. Different loading of Fe (0.1 wt%, 0.2 wt%, 0.4 wt%, 0.6 wt%, 0.8 wt% and 1.0 wt %) with the calcination temperature of 350^oC, 400^oC and 450^oC are investigate throughout the experiment. The calcination temperature, synergic effects of particle size and surface area play an important role in desulfurization.

Acknowledgment

First and foremost, I would like to express my gratitude to God for His kind blessings by giving me the strength and determination to complete this Final Year Project 2 course after stressed with all the difficulties and challenges for the past several months.

I would also like to take this opportunity to express my utmost gratitude to Universiti Teknologi PETRONAS (UTP) for providing me with all the facilities to complete my project within stipulated time. I would like to direct my highest gratitude to my supervisor and co-supervisor, Prof. T. Murugesan and Associate Professor Dr. Chong Fai Kait for all their guidance and continuous support throughout the semester. They have been very supportive supervisor and willing to share their knowledge, in order to ensure that I could learn and understand every single thing in this project.

My gratitude is also extended to a PhD student, Mrs Hayyiratul for her effort in assisting me in all the possible ways. She has always leaded me, gave advice and explained the problems associated with my project providing me with the necessary materials and analysis laboratory work. She has helped me to gain useful experience and knowledge needed for the project.

Last but not least, my appreciation is given to all the staff members in the ionic liquid station, centralized analytical laboratory (CAL), mechanical engineering department and chemical engineering department for their contributions and equipment which helped me a lot to make sure that this project ended successfully.

Table of Contents

List of Figure

List of Table

1 Introduction

1.1 Background

Diesel oil has become one of the main fuels for automobile. The diesel market has been growing significantly over the years as diesel vehicles could perform better than gasoline-powered vehicles. According to Energy Information Administration (EIA) forecast, by 2023 the consumption of diesel would be more than 17.1% and 26.0% more by 2014 (NACS, 2014). With the increasing in diesel consumption, the main pollution which is sulfur by-product is gradually increasing. These sulfur species are classified into mercaptans (thiols), sulfides, disulfides and thiophenes. Stringent environment standard has enforced the sulfur content of diesel oil.

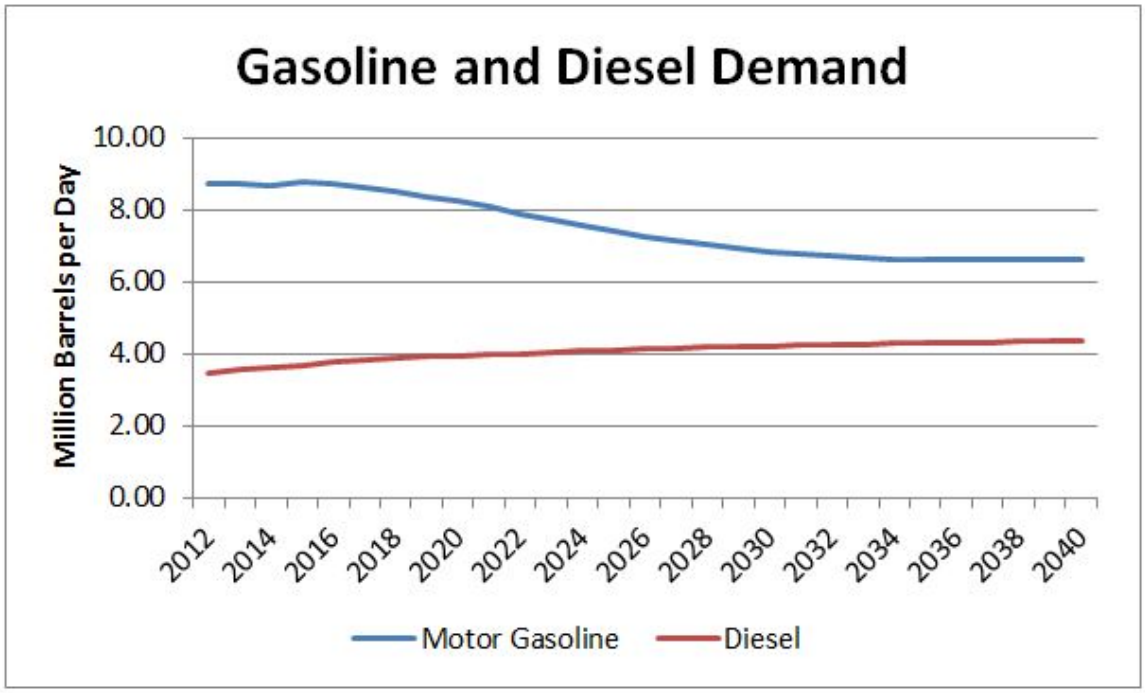

Figure 1-1 Demand of gasoline and diesel as time growth

The high level of exposure to sulfur in the environment has directly increase the pollution or health effect of the people. Exposure to a certain level of sulfur dioxide can cause to health problems such as respiratory effects, eye irritation, headache, immune system problems, cancer risk and asthma. National Institute for Occupational Safety and Health (NIOSH) and Occupational Safety and Health Administration (OSHA)

recommended that the exposure limit of sulfur dioxide is 5ppm for 15 minute period and 2ppm for an 8-hour time weighted average.

Currently, the sulfur content for diesel in Malaysia is 500ppm which is Euro II-equivalent standard (Singh, 2009). June 1, 2015 is the roll-out date for Malaysia to increase the standard of Euro II to Euro V, which has decrease the sulfur content from 500ppm to 10ppm. Table 1-1 below shows the standard of sulfur content (ppm) in diesel oil.

With the current technology of desulfurization of diesel which is hydrodesulphurization (HDS) method is not effective for removing sulfur component with high stearic hindrance. HDS process uses Co-Mo/Al_2O_3, Ni-Mo/ Al_2O_3 or Ni-W/ Al_2O_3 as catalyst

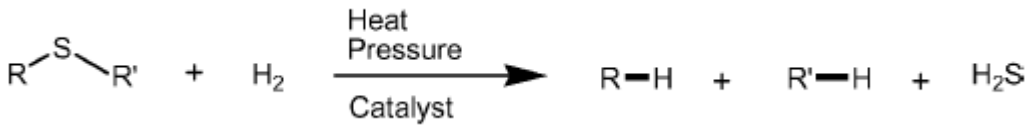

Figure 1-2 removal of sulfur compound by HDS process

for converting sulfur component to H_2S. Besides, this process need to be operate at high temperature (300-400^oC) and pressures (20-100atm of H_2) and this has led to high operating cost. It is effective in removing thiols, sulfides and thiophenes but less effective for benzothiophene, dibenzothiophene and their alkyl derivative (Kulkarni & Afonso, 2010).

Due to high concern of sulfur dioxide, there is an abundance of researches or ways to remove sulfur such as photo-oxidative desulfurization, oxidative desulfurization, bio-desulfurization, reactive adsorption, nondestructive adsorption, N-adsorption, extraction, and miscellaneous processes (Kulkarni & Afonso, 2010).

Table 1-1 Types of Diesel Sulfur Content

Standard	**Sulfur content (ppm)**
Euro II (Low Sulfur Diesel)	500
Euro IV (Ultra Low Sulfur Diesel)	50
Euro V (Green Diesel)	10
Euro VI (Very Low Sulfur Diesel)	<5

1.2 Problem Statement

This project is related to the deep desulfurization of diesel oil under visible light using TiO_2 followed by impregnation of Fe in visible light condition. Presently, HDS process is used to eliminate sulfur compound in the condition of high pressure and temperature. This shortcoming process has increased the cost of operation as well as its limitation in refractory sulfur species. The adverse effect from sulfur species has raised concern to the public. In order to improve the desulfurization of diesel oil, photocatalyst is employed. This is the ultimate aim of this research which is to study the effect of metal on deep desulfurization of diesel oil using Fe/TiO_2 under visible light radiation. The kinetic study of desulfurization with the different reaction conditions and additional metal ion would be analyzed throughout the experiment.

1.3 Objectives

The main objectives of the study are:

- To prepare Fe/TiO_2 photocatalyst which is active in visible region
- To characterize Fe/TiO_2 photocatalyst
- To shift the active region of photocatalyst from UV to visible region

1.4 Scope of Study

In this experiment, photocatalyst, Fe/TiO_2 was synthesized to compare or to investigate the kinetics of photocatalysis with some key influencing factors. The characteristics of the TiO_2 were then analysed for their synergy effect of particle size, surface area and the transparency. The effect of different operating parameters on the:

a) Photocatalyst with different weight percentage of metal loading
b) Calcination temperature and duration.

2 Literature Review and/or Theory

2.1 Photocatalyst

There is variety of researches on the methods of diesel oil desulfurization. The most effective and well-known for removal organic components is titanium dioxide photocatalysis. TiO_2 with a light source, UV is used to initiate the photoreaction. UV could differentiate into 3 type of UV which is UVA, UVB and UVC. The wavelength of UVA is between 320nm to 400nm which is next to the visible light (400nm-700nm). The radiation of UVB is from 280 nm to 320 nm and between 200 nm and 280 nm is UVC (Moan, 2001).

From the *Figure 2-1* and *equation 1*, with the present of light source, the electron at valence band has the tendency to lose its electron to form free electron that could bind at the conduction band (Rao, D.G. et al, 2012). The gap between valance band and the conduction band is called energy gap or bond gap. The hole will generate hydroxyl radicals, •OH (equation 2 and 3) and act as an oxidizing agent to oxidize organic component.

Source: Rao, D.G. et al, 2012

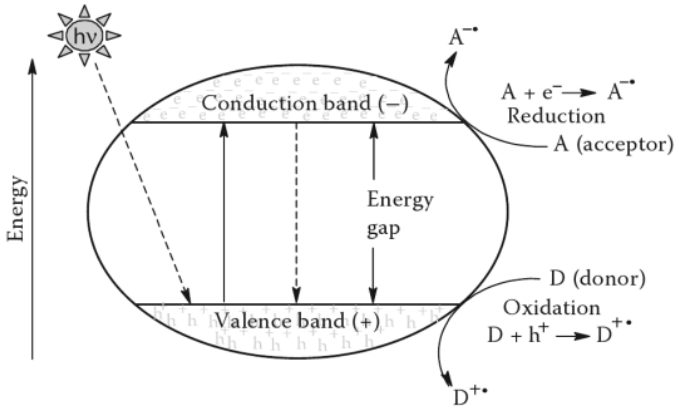

Figure 2-1 Principle of Photocatalyst

$TiO_2 \xrightarrow{hv} TiO_2(e_{CB}^- + h_{VB}^+)$ Equation 1

where CB is conduction band and VB is the valence band

$h^+ + H_2O \rightarrow \bullet OH + H^+$ Equation 2

$h^+ + -OH \rightarrow \bullet OH$ Equation 3

Characteristic of TiO_2 plays an important role in photodegration. For example, the surface area, active sites, absorption of photon energy and band gap energy have the function of effecting the organic component degradation (Al-Rasheed, 2005). Besides, TiO_2 could synthesis by $TiCl_4$ with the additive H_2SO_4 which could composed TiO_2 in anatase phase (Li & Zeng, 2011). They claimed that high concentration of sulfuric acid can increase the crystallinity. Serially, slightly higher ratios of water also rise up the crystallinity. The calcination temperature is important as it could affect the particle size.

Based on Sarda, Bhandari, Pant, & Jain, 2012, they argued that addition of Ni and Cu on active carbon and zeolite support could performance better than other metal supported on zeolite. The use of H_2O_2 in desulfurization is slightly improving the performance of photocatalyst and due to the presence of oxidant. However, the flow rate and bed height could affect the performance in removing the sulfur species. Thus, new method should be implying for the improvement performance of photocatalyst.

In the diesel oil, a variety of sulfur species are present including:

i. aliphatic molecules such as sulfides, disulfides, and mercaptans,
ii. aromatic molecules such as thiophene, benzothiophene, dibenzothiophene,
iii. alkyl derivatives such as 4,6-dimethyl-dibenzothiophene

With the current HDS process, converting refractory sulfur components such as dibenzothiophene (DBT) into H_2S is less competent due to the steric hindrance on the catalyst surface. Thus, HDS is required to operate at condition of high temperature and pressure as well as a larger reactor with an active catalyst. The alternative strategies replace current deep desulfurization are include oxidative desulfurization, bio-

desulfurization, reactive adsorption, extraction by using ionic liquid, and other various processes (Kulkarni & Afonso, 2010).

Abundance researches on removing sulfur component by using ionic liquid extraction showed the potential of achieving low sulfur concentration in diesel. An ionic liquid is a non-volatile organic salt in liquid phase. It has a broad range of applications which has potential to use its polarity for removing sulfur and organic nitrogen compounds in fuels under mild condition. There are few types of IL that are current use in deep desulfurization. For example, imidazolium-based ionic liquids, pyridinium-based ionic liquids, Lewis and Brønsted acidic ionic liquids or redox ionic liquids (Kulkarni & Afonso, 2010).

2.2 Ionic Liquid

A. Imidazolium-based ionic liquids

Mochizuki & Sugawara, (2008) used six types of halogen- free ionic liquids imidazolium sulfate such as 1,3-dimethylimidazolium methyl sulfate ($MMIMMe^+SO_4^-$), l-ethyl-3-methylimidazolium ethyl sulfate ($EMIMET^+SO_4^-$), l-ethyl-3-methylimidazolium ethyl sulfate ($EMMMe^+SO_4^-$), l-ethyl-3-ethylimidazolium ethyl sulfate ($EEIMET^+SO_4^-$), l-butyl-3-methylimidazolium methyl sulfate ($BMIMMe^+SO_4^-$) and l-butyl-3-ethylimidazolium ethyl sulfate ($BEIMEt^+SO_4^-$). Dibenzothiophene (DBT) was extracted at room temperature using six types of halogen-free ionic liquids. The increase of carbon number of alkyl group in IL can increase the extraction of dibenzothiophene. The extractive performance using imidazolium based ILs followed the order $BEIMEt^+SO_4^-$> $EEIMET^+SO_4^-$> $BMIMMe^+SO_4^-$ > $EMIMET^+SO_4^-$ > $EMMMe^+SO_4^-$ > $MMIMMe^+SO_4^-$. After five rounds of repeating extractions, the level of sulfur could be decreased from 1000ppm to 350ppm.

B. Pyridinium-based ionic liquids

Another way to extract sulfur species is through pyridinium-based ionic liquids. N-alkyl-pyridinium-based ionic liquids, N-butyl-pyridinium nitrate ([BPy]NO_3), N-ethyl-pyridinium nitrate ([EPy]NO_3), N-butyl-pyridinium tetrafluoroborate ([BPy]BF_4), N-ethyl-pyridinium tetrafluoroborate ([EPy]BF_4), N-ethyl-pyridinium acetate ([EPy]Ac), and N-butyl-pyridinium acetate ([BPy]Ac) is selected to desulfurize the model oil (Wang, Zhao, Zhou, & Dong, 2007). The increase in mass ratio of ILs to the model oil (1:1), [BPy]BF_4 showed the best absorption thiophene capacities from the model oil among the six ILs. Also, it concluded that with the increase of mass ratio of ILs to the model oil has the more ability to extract thiophene. The cation or anion structure and the size of ILs play an important role as it could affect the ability of sulfur extraction. The temperature on the desulfurization can deflect the viscosity of ILs. As temperature increase, the viscosity of ILs is reduced and it high retention time to contact with sulfur species in the model oil. This will result in the high sulfur removal.

C. Lewis and Brønsted acidic ionic liquids

Zhao, Wang, & Zhou, (2007) used the Brønsted acid IL with the presence of H_2O_2 to desulfurize diesel fuel. H_2O_2 act as the oxidative agent as it could enhance the performance of converting sulfur species to their corresponding sulfones. The percentage of removal sulfur increase as the molar ratio of H_2O_2/ sulfur increase. They also tested that Brønsted acid IL need to be operated at a higher temperature to achieve 100% conversion of DBT within 1 hour. Besides, the ionic liquid [Hnmp]BF_4 can be recycled and act as catalyst and extractant. As it has reduced the viscosity of IL for the purpose of increasing the contact time with the sulfur species in diesel oil. It also showed that 7 times of recycling would not significantly decrease in activity. The percentage of sulfur removal remaining 93.4% as the recycle of [Hnmp] BF_4.

2.3 Photo-oxidative extraction deep desulfurization

Photo-oxidative extractive is a photocatalytic oxidation which is significant research interest due to its high efficiency and simplicity. The photo-catalytic oxidation desulfurization using the presence of ultraviolet irradiating to activate TiO_2 as the photo catalyst (Wang, Cai, Lia, & Mominou, 2013). Photocatalyst was added to model oil to be oxidized under visible light after which it will be extracted using ionic liquid under room temperature and pressure. A high pressure mercury lamp of visible light is used to oxidize the sulfur compounds in diesel and the sulfur compounds can be extracted by ionic liquids (ILs). However, the sulfur removal efficiency with ILs is quite low because of the similar polarity between the sulfur-containing molecules and remaining diesel fuels (Zhang, et al., 2012).

3 Methodology/Project Work

3.1 Project Flow Chart

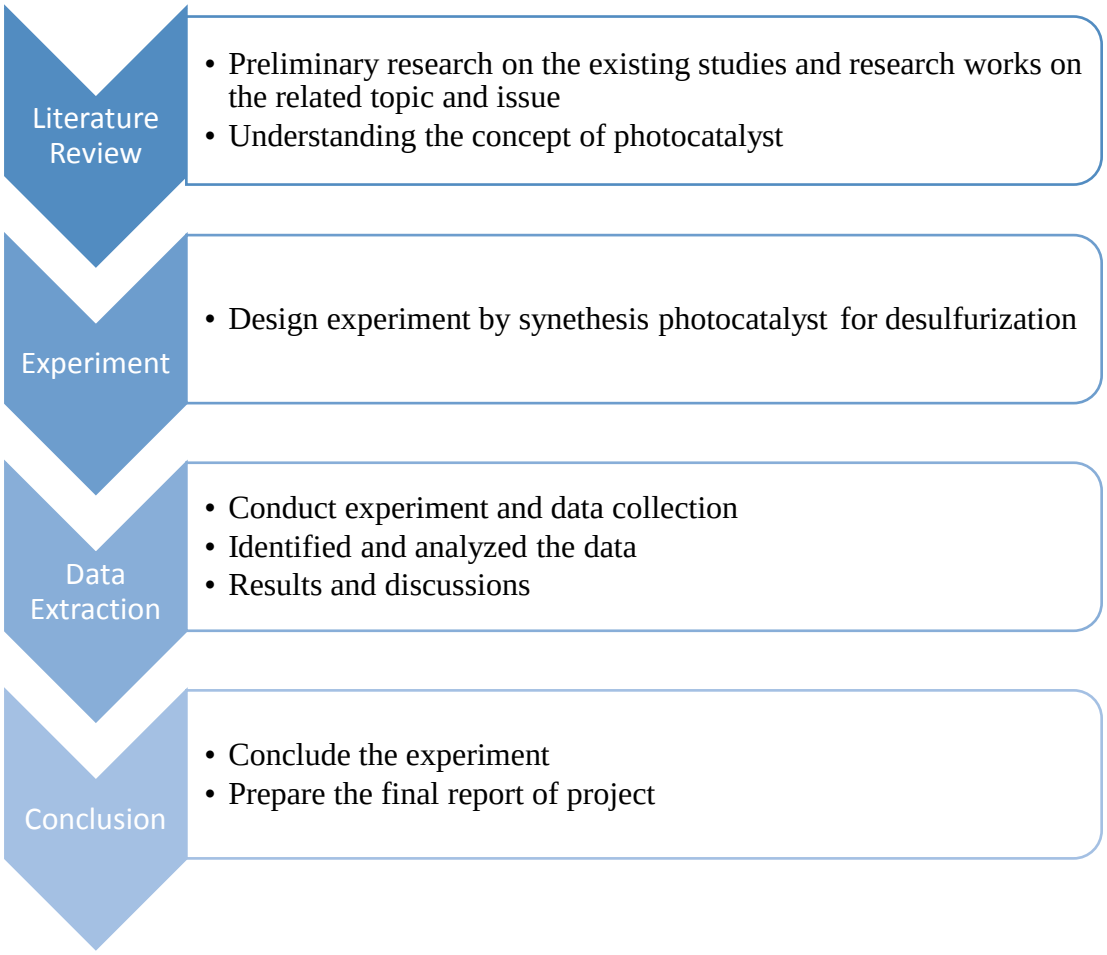

3.2 Key milestone/Gantt Chart

Table 3-1Gantt chart for final year project 2

No.	Detail	1	2	3	4	5	6	7	8	9	10	11	12	13	14
1	Project Work Continues	■	■	■	■	■	■	■							
2	Submission of Progress Report							★							
3	Project Work Continues								■	■	■	■	■		
4	Pre-SEDEX										★				
5	Submission of Draft Final Report											★			
6	Submission of Dissertation (soft bound)												★		
7	Submission of Technical Paper												★		
8	Viva													★	
9	Submission of Project Dissertation (Hard Bound)														★

★ Key milestones

■ Activities

3.3 Proposed Experiment Procedure

Figure 3-1 shows the schematic diagram of the overview of Fe/TiO_2 photocatalyst preparation.

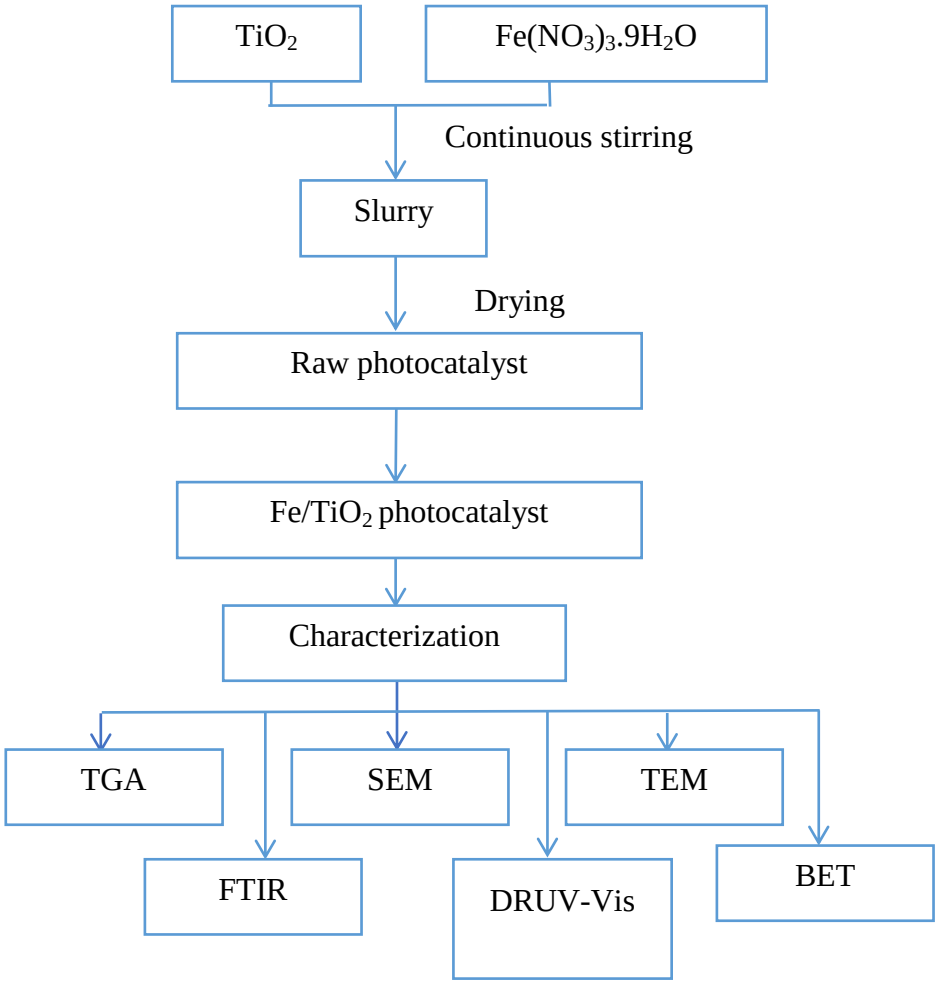

Figure 3-1 Overview of Fe/TiO_2 photocatalyst preparation

1) Preparation of Fe/TiO_2

A series of Fe/TiO_2 photocatalysts were prepared on the composition required, temperature and duration of calcination using wet impregnation method. Iron(III) nitrate nonahydrate ($Fe(NO_3)_3.9H_2O$) was used as the Fe precursor for the photocatalyst preparation. The Fe loading was investigated in this project are 0.1 wt%, 0.2 wt%, 0.4 wt%, 0.6 wt%, 0.8 wt% and 1.0 wt%. A pretermined amount of TiO_2 (Degussa P25, 80% anatase, 20% rutile; 20-50nm diameter) was suspended in 300ml distilled water. Subsequently, Fe^{3+} (aq) solution was added slowly into the TiO_2 slurry with continuous stirring. Then, the solvent was evaporated in as water bath at 80^oC, followed by dried at 120^oC for 15 hours. In order to activate the raw photocatalyst, calcination

process was conducted at 350°C, 400 °C, 450 °C and 500 °C for 0.5 h and 1 hr. Photocatalyst with different Fe loading were investigated.Table 3-2 summarizes the amount of Fe used to prepare the photocatalysts. Appendix A showed the calculation of the photocatalyst. The calculations involved are shown in Appendix A.

Notation: 0.1Mg400_1 means 0.1 wt% of iron doped on TiO_2 calcined at 400°C and 1 h only.

Table 3-2 Summary of the Fe Loading for Wet Impregnation

Fe Loading, %	**Mass of TiO_2 Precursor**	**Mass of $Fe(NO_3)_3.9H_2O$ Required to Produce 100g of Fe/TiO_2 with Different Loading**
0.1	99.2769	0.7231
0.2	98.5538	1.4462
0.4	97.1075	2.8925
0.6	95.6613	4.3387
0.8	94.2151	5.7849
1.0	92.7688	7.2312

2) Characterization of Fe/TiO_2

Characterization of the samples was carried out to determine the physical and chemical properties of the photocatalysts. The overview of the photocatalyst characterization is shown in Figure 3-2.

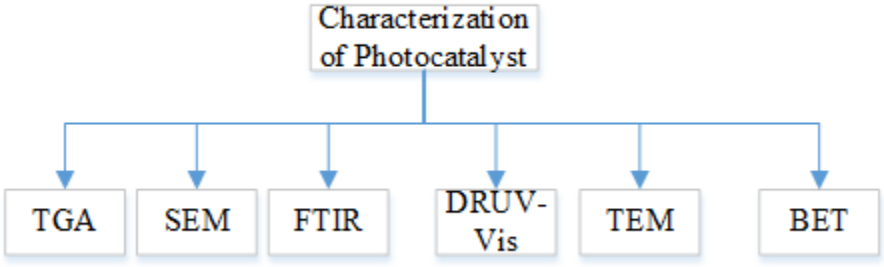

Figure 3-2 Overview of Photocatalyst Characterization

Thermal Gravimetric Analysis (TGA)

Thermal gravimetric analyses (TGA) were carried out using Perkin Elmer TG (Pyris 1) system to determine the approximate decomposition temperature of the raw material of Fe/TiO_2. The samples were weighed in the range of 2-5 mg using a built-in microbalance attached in the instrument which automatically read the weight of the sample. The samples were heated from 50°C to 850°C at a ramp rate of 10°Cmin-1.

Fourier Transform Infrared Spectroscopy (FTIR)

Fourier Transform Infrared Spectroscopy (FTIR) is used to identify functional groups present in the samples. The FTIR spectra of the Fe/TiO_2 catalysts with various calcination temperatures were scanned from 4000 cm^{-1} to 450 cm^{-1} by Perkin Elmer Spectrophotometer. Approximately 1 mg of each powder sample was grained with 200 mg to 300 mg of KBr. The samples were then transferred into a die and were pressed into a pellet using a hydraulic hand press. The pellet was transferred and placed in a sample holder and scanned using the FTIR instrument. During the analysis, some of the infrared radiation was absorbed and some of it was passed through the sample. The molecular absorption and transmission are shown in the spectrum result in the form of functional group fingerprint which could be identified by the characteristics peaks in the spectrum.

Scanning Electron Microscope with Energy Dispersive X-ray (SEM/EDX)

The morphology and size distribution were evaluated through scanning electron microscope (SEM). The samples were scanning at 5,000X magnification where it could magnification from 20X to approximately 30,000X and spatial resolution of 50 to 100 nm. The SEM micrographs are expected to generate a variety of signals at the surface of Fe/TiO_2 specimens. The signals that derive from electron-sample interactions reveal information about the sample including external morphology, texture, chemical composition, and orientation of materials making up the sample (Swapp, 2013). The SEM is also capable to perform analysis on selected point locations. By using the function of EDX mapping, it could determine the chemical components in qualitatively or semi-quantitatively.

Transmission Electron Microscopy (TEM)

Crystal structure, lattice constraints and specimen orientation were determined by Zeiss Libra 200. TEM specimen stage includes airlocks to allow for insertion of the specimen holder into the vacuum with minimal pressure increase. Once the photocatalyst is inserted into TEM, the sample has to be manipulated to present the region of interest to the beam. The magnification is 200kV giving us the size and shape of the particles.

Diffuse Reflectance UV-visible spectra (DRUV-Vis)

The absorbance and diffuse reflectance of the photocatalyst were analyzed by Agilent Cary instruments. The sample was placed in the sample holder and make sure the sample holder is fully covered. Then, the sample holder is placed at correct cell position for analysis. The absorption edge, band gap energy, and the type of band to band transition of TiO_2 were obtained from these spectra. The reflectance spectra were used to calculate remission function, F(R) = (1-R)2/2R (based on the Kubelka-Munk theory or diffuse reflectance). The band gaps for all the photocatalysts were determined from the extrapolation of the absorption edge onto the energy axis (Eg).

Brunauer-Emmette-Teller (Surface Area & Porosity)

Micromeritics ASAP 2020 is used to measure the adsorption and desorption isotherms for characterization of surface area, pore size, pore volume and mesoporous materials. Surface area of photocatalyst is influenced by particle size as it could affect the performance of photocatalyst. The surface charge carrier transfer rate in photocatalysis increase as the result of increasing avtive surface sites which has a smaller particle size (Zhang, Wang, Zakaria, & Ying, 1998).

4 Results and Discussion

4.1 Characterization of Fe/TiO_2 photocatalyst

4.1.1 Thermal Gravimetric Analysis (TGA)

To investigate the thermal behaviour of the uncalcined Fe/TiO_2 photocatalysts, a thermal gravimetric analysis (TGA) was performed before the catalysts are being sent into the furnace for calcination. Thermal treatment (calcination) is carried out in order with the aim of decompose some compounds present in the catalyst. With calcinations process, the physical and chemical properties of catalysts, especially porous structure and mechanical strength will be induced in the degradation process. Figure 4-1 and Figure 4-2 show the TGA analysis of different doping of Fe on TiO_2 and raw material of TiO_2 and $Fe(NO_3)_3$. From the Figure 4-2, the TGA analysis of $Fe(NO_3)_3.9H_20$ shows 3 stages of decomposition. It shows a slow weight loss from room temperature to 140°C, at which an accelerated loss of weight occurred until 400°C and it shows no changes after 400°C. The first weight loss step occurred between 48°C to 140°C depicts the removal of water. The intense weight loss between 140°C to 170°C depicts the possible decomposition of $Fe(NO_3)_3$ (Bin Li, Shi, Ye, Wu, & Zhao, 2013); (Fassier, Peyratout, Smith, Ducroquetz, & Voland, 2010).

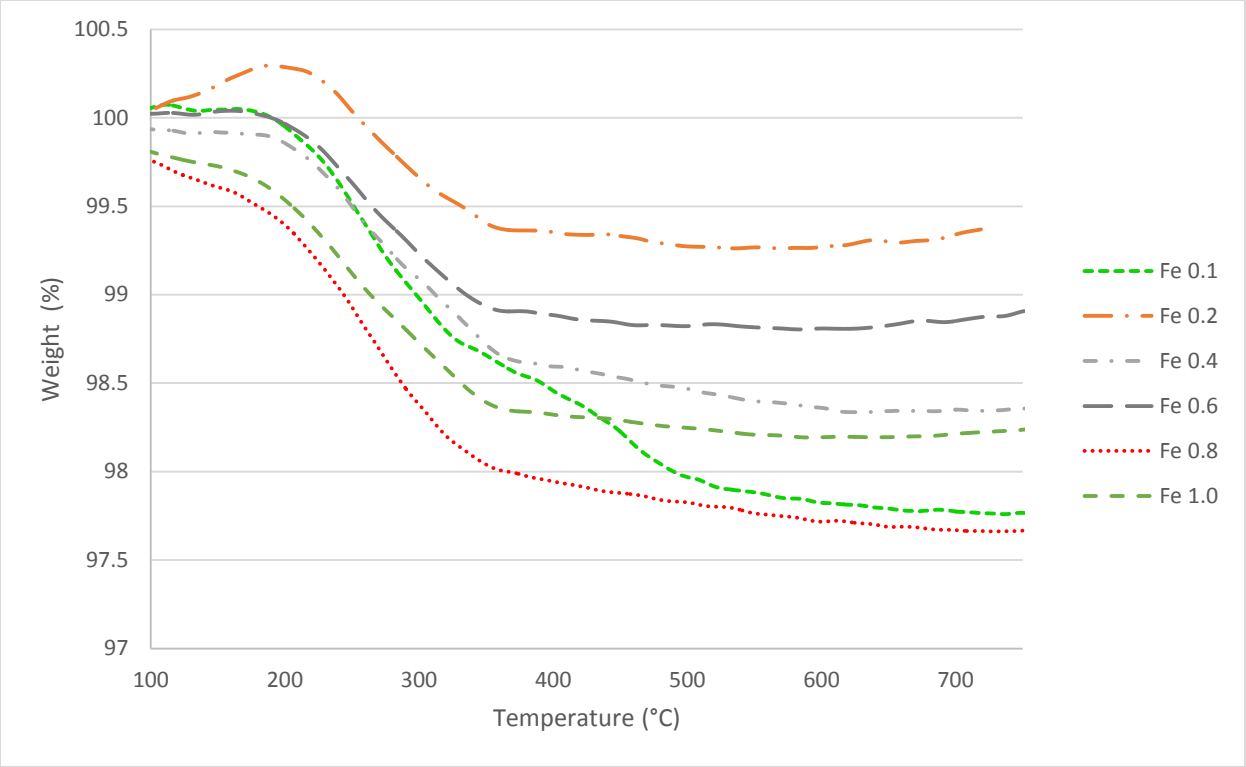

Figure 4-1 TGA analysis of raw Fe/TiO_2 photocatalyst

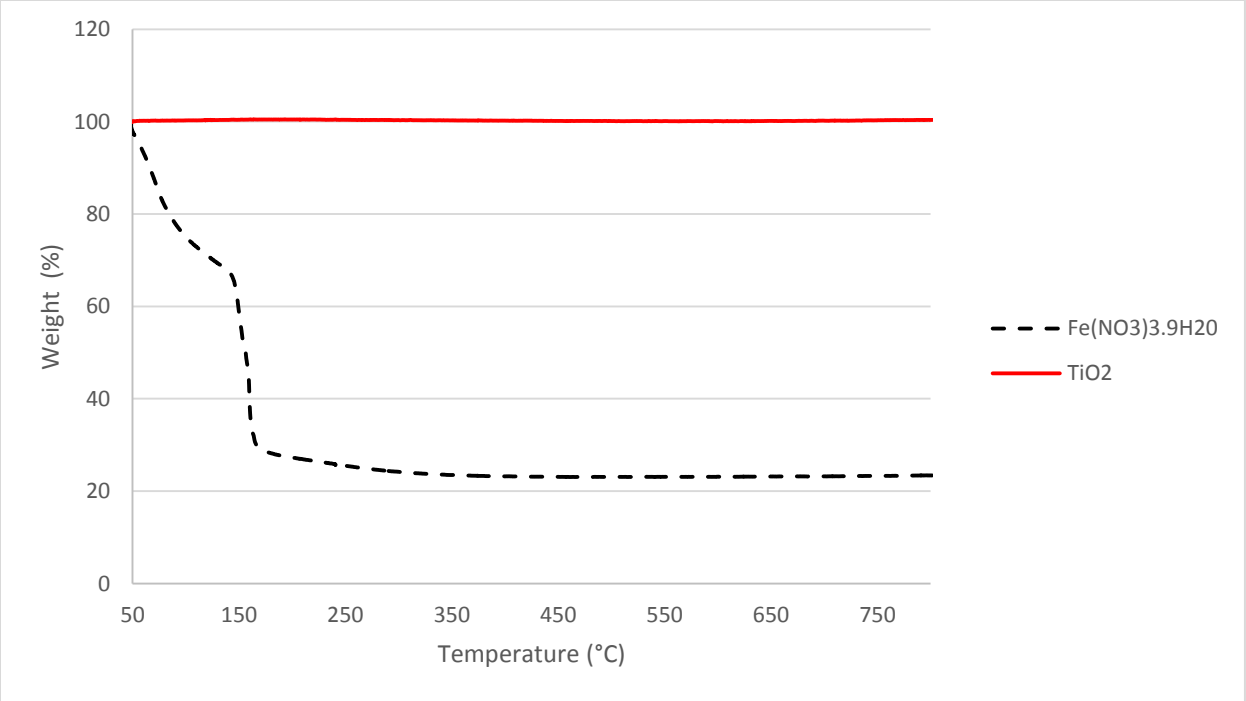

Figure 4-2 TGA analysis of raw material TiO_2 and $Fe(NO_3)_3.9H_20$

4.1.2 Fourier Transform Infrared Spectroscopy (FTIR)

Figure 4-3 showed the FTIR transmission spectra of different loading of Fe on TiO_2 which are calcined at 400°C for 1 hour and the uncalcination of 0.2 wt% of Fe doping for comparison purpose. From the spectra shown in Figure 4-3, the absorption peak around 1600 cm^{-1} and 3400 cm^{-1} were attributed to the O-H bending and stretching, correspondingly (Li, Haneda, Hishita, & Ohashi, 2005). The other peak around 1384cm^{-1} showed the presence of nitrate functional group (Niu, Qing, & Kaibin, 2006). However, after calcination the presence of nitrate functional group were no longer present. This implies that the nitrate functional group is completely removed during the calcination process. The other absorption peak between 400–900 cm^{-1} corresponds to the Ti-O stretching vibrations (Linacero, Aguado-Serrano, & Rojas-Cervantes, 2006); (Porkodi & Arokiamary); (Yan, He, Evans, Zhu, & Duan, 2004). The FTIR spectrums of different loading of Fe with different calcination temperature are shown in Appendix C.

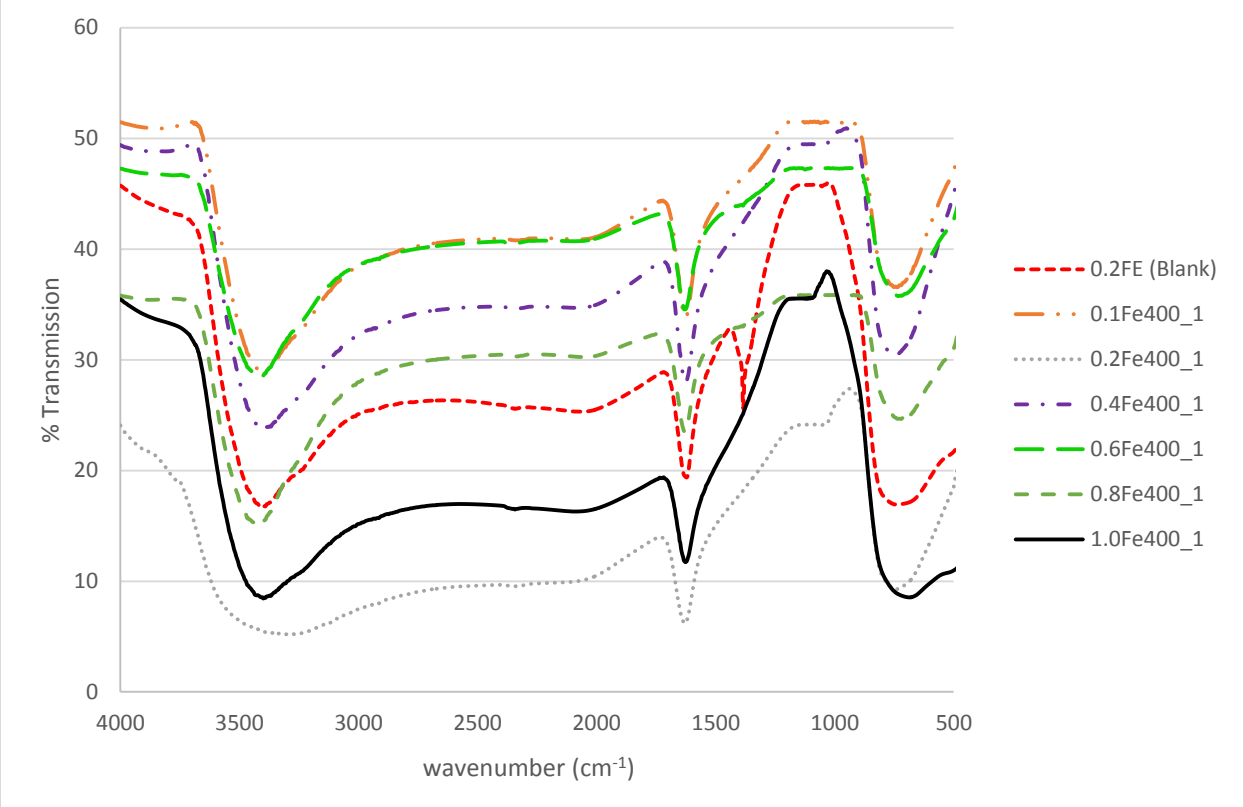

Figure 4-3 FTIR result with different loading of Fe and raw Fe/TiO_2 photocatalyst

4.1.4 Scanning Electron Microscope/Energy Dispersive X-ray (SEM/EDX)

SEM is used to determine the morphology of the Fe/TiO_2 photocatalysts. The samples were scanning at 20kX magnification. Figures and tables below show morphologies and chemical composition of 0.1 wt%, 0.2 wt%, 0.4 wt%, 0.6 wt%, 0.8 wt% and 1.0 wt% of Fe doping on TiO_2 with the calcination at 400^oC. From the EDX analysis, there is a big difference between the calculated Fe and analysis Fe. This is due to poor maintenance of SEM equipment.

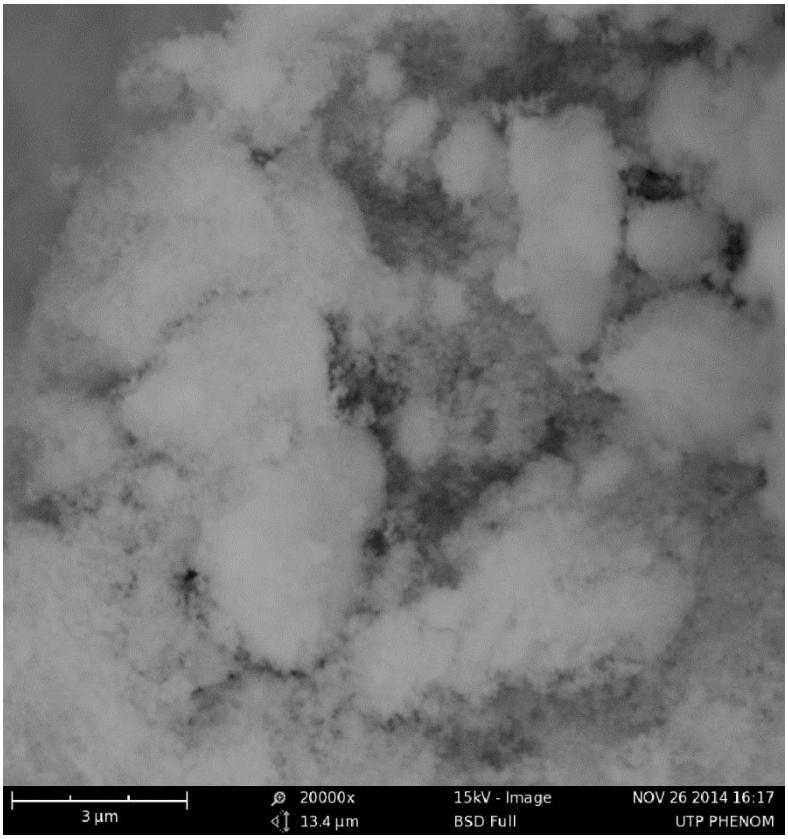

Figure 4-4 SEM micrographs of 0.1Fe400_1 at 20k× magnification

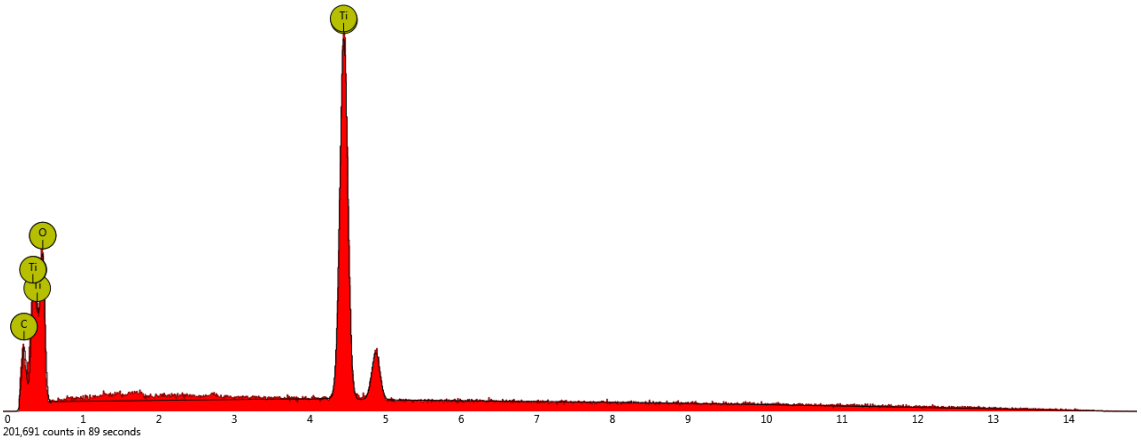

Table 4-1 EDX mapping of 0.1Fe 400_1

Element	% Mass
Ti	31.7
O	66.7
C	1.6
Fe	0.1

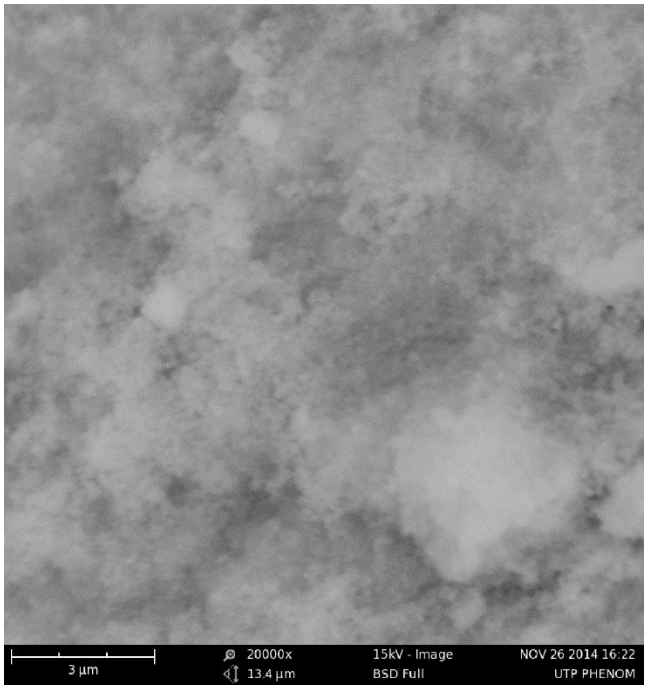

Figure 4-5 SEM micrographs of 0.2Fe 400_1 at 20k× magnification

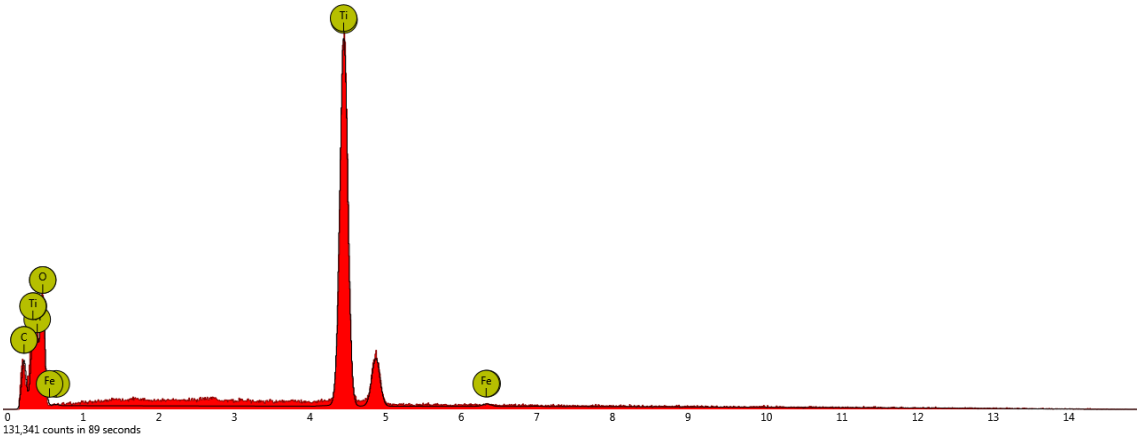

Table 4-2 EDX mapping of 0.2Fe400_1

Element	% Mass
Ti	36.7
O	61.3
C	1.5
Fe	0.6

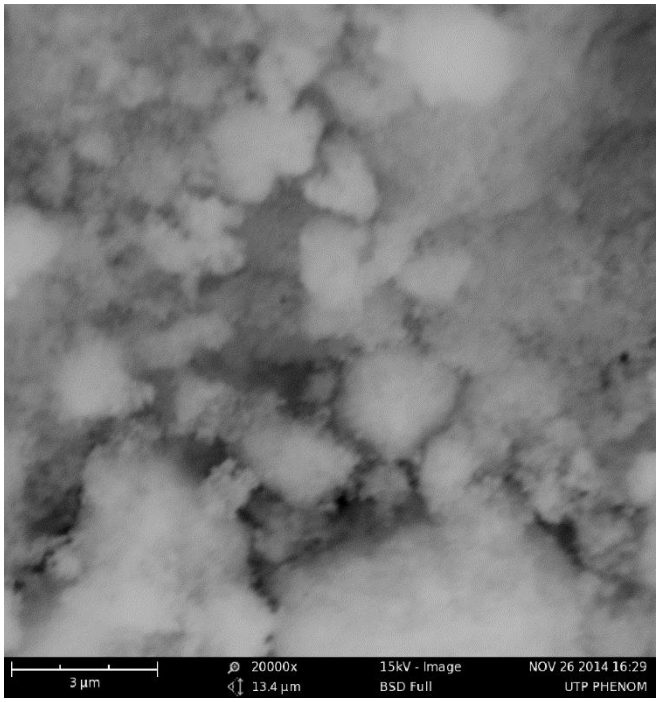

Figure 4-6 SEM micrographs of 0.4Fe400_1 at 20k× magnification

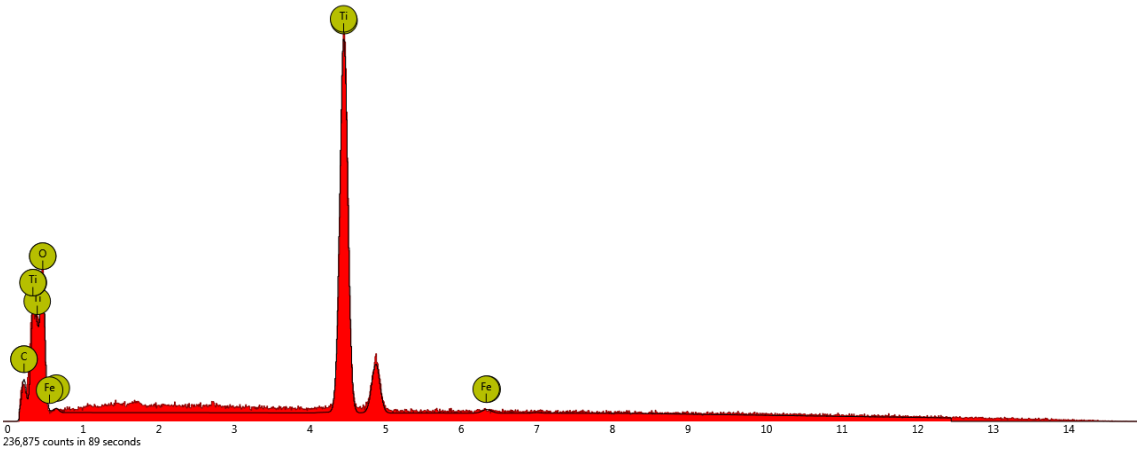

Table 4-3 EDX mapping of 0.4Fe400_1

Element	% Mass
Ti	33.2
O	65.1
C	1.0
Fe	0.7

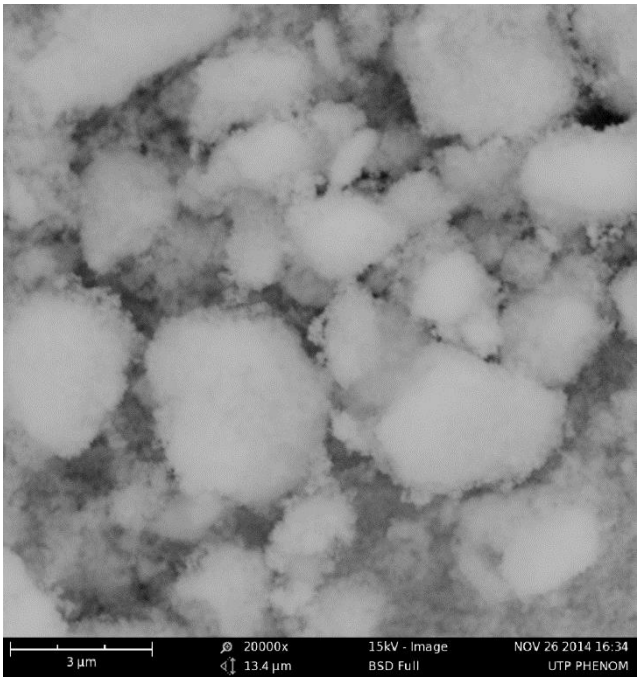

Figure 4-7 SEM micrographs of 0.6Fe 400_1 at 20k× magnification

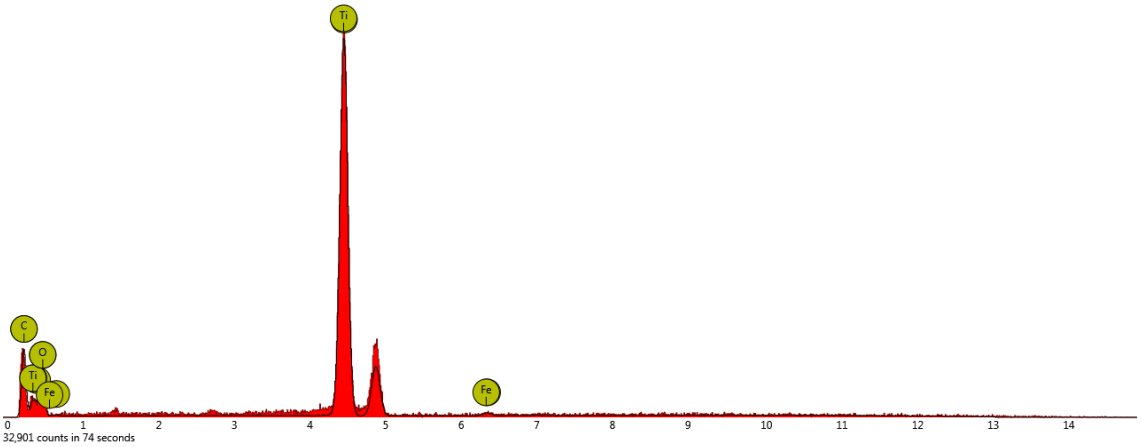

Table 4-4 EDX mapping of 0.6Fe 400_1

Element	% mass
Ti	51.6
C	3.1
O	44.3
Fe	0.9

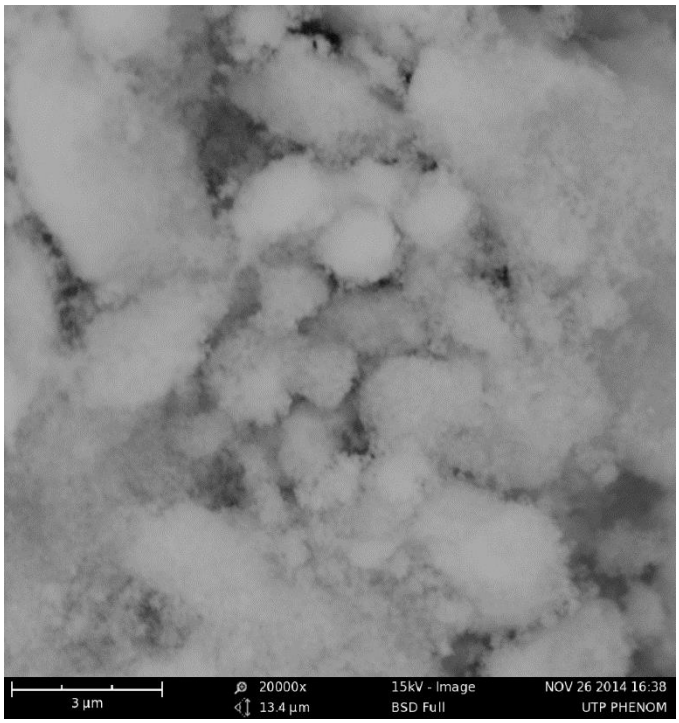

Figure 4-8 SEM micrographs of 0.8Fe400_1 at 20k× magnification

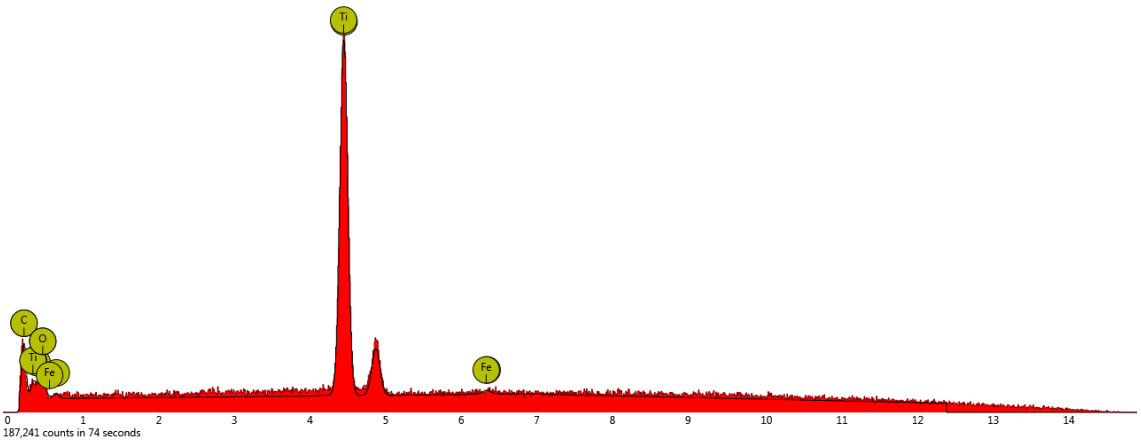

Table 4-5 EDX mapping of 0.8Fe400_1

Element	% mass
Ti	52.4
C	2.8
O	43.8
Fe	1.0

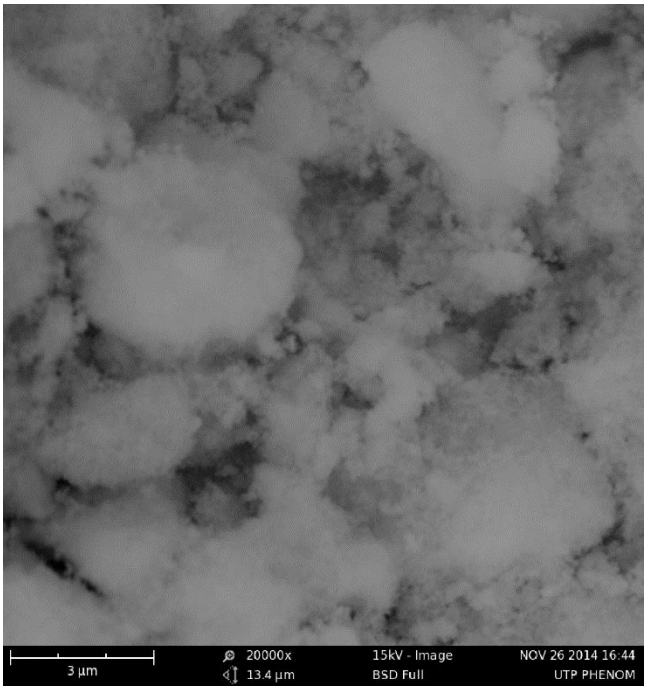

Figure 4-9 SEM micrographs of 1.0Fe400_1 at 20k× magnification

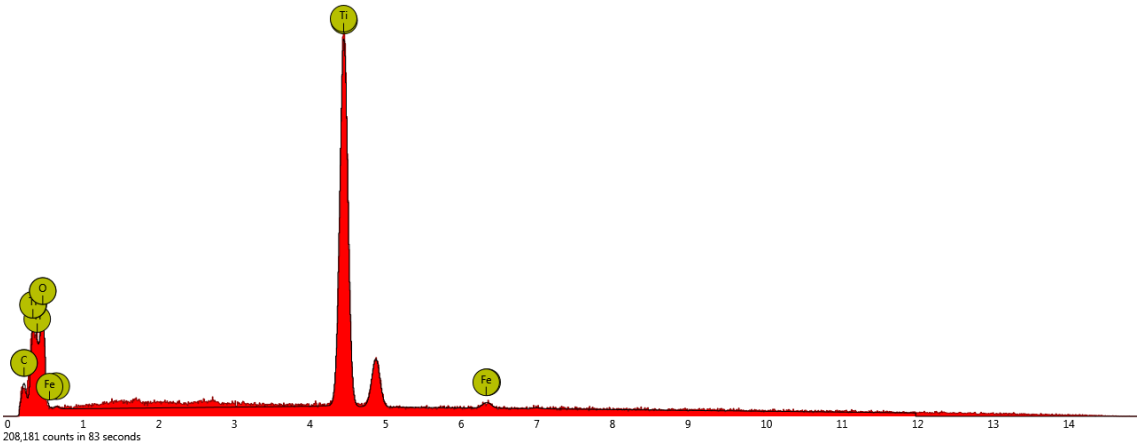

Table 4-6 EDX mapping of 1.0Fe400_1

Element	% mass
Ti	37.8
O	60.1
C	0.9
Fe	1.3

4.1.5 Transmission Electron Microscopy (TEM)

Transmission Electron Microscopy (TEM) is an analytical device allowing visualization and analysis of specimens in the realms of microspace to nanospace by transmitting a beam of electrons through an ultra-thin specimen (Background information - What is transmission electron microscopy, 2013). An image is formed from the interaction of the electrons transmitted through the specimen, whereby the image is magnified and focused onto an imaging device. TEM are capable of imaging at a significantly higher resolution and high magnification. This enables the examination of the fine detail-even as small as a single column of atoms. TEM gives clearer morphologies, crystal structures and specimen orientations of the photocatalyst.

From the figures below, the TEM images showed that there are two different spaces between the fridges. This could mean that there are presence of iron and titanium which are of different particles in it. The lattice fringes of 0.2Fe400_1 are 0.361 nm and 0.5947 nm. According to Matei, Predescu & Vasole (2011), 0.361 nm can be assigned as (101) plane which is contribute to anatase of TiO_2. Besides, Figure 4-13 showed the d-spacing of 0.3488 nm and 0.1481 nm which assigned to (101) plane of TiO_2 and (440) plane of Fe_2O_3 respectively (Kundu & Chakravorty, 1999); (Matei, Predescu, Predescu, Vasile, & Predescu, 2011).

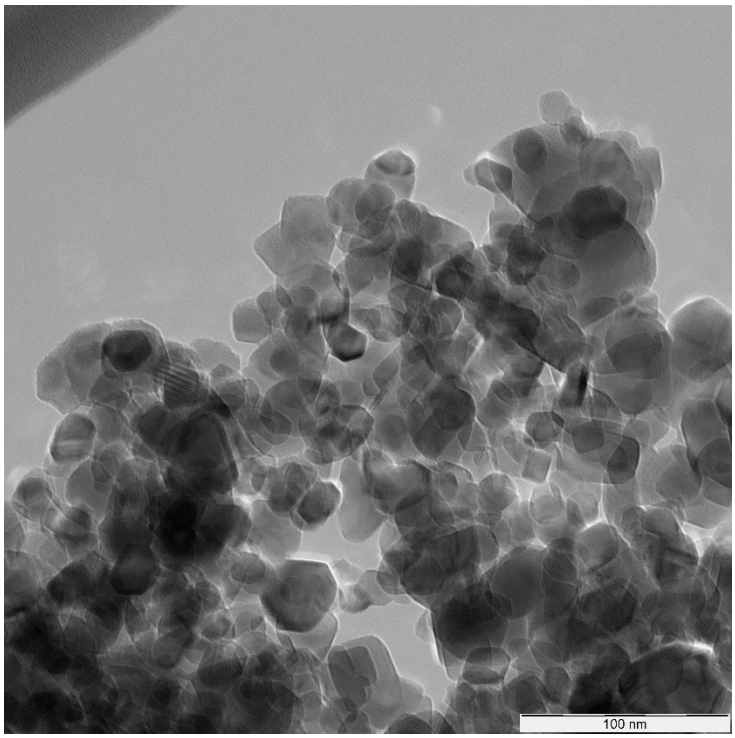

Figure 4-10 TEM micrographs of 0.2Fe400_1

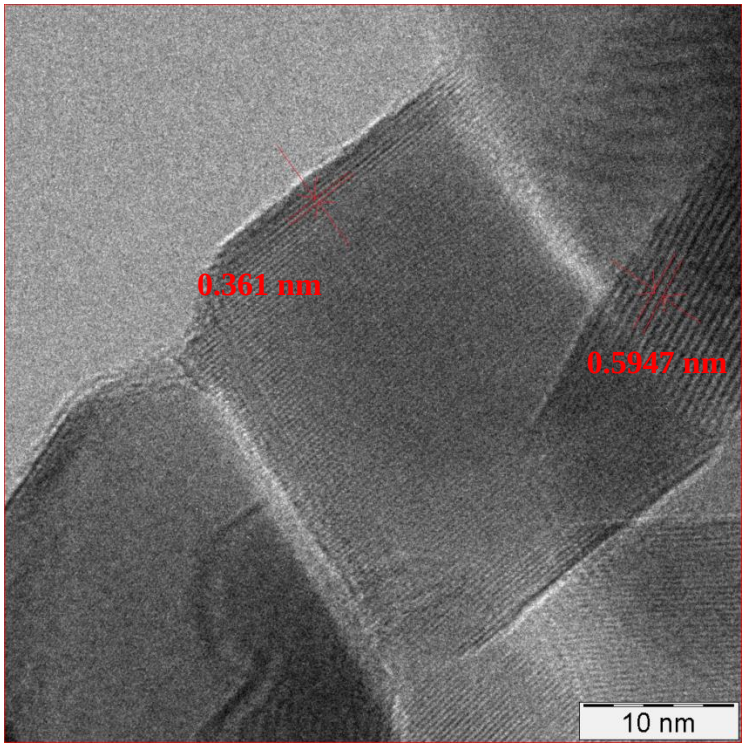

Figure 4-11 Fringes of the 0.2Fe400_1

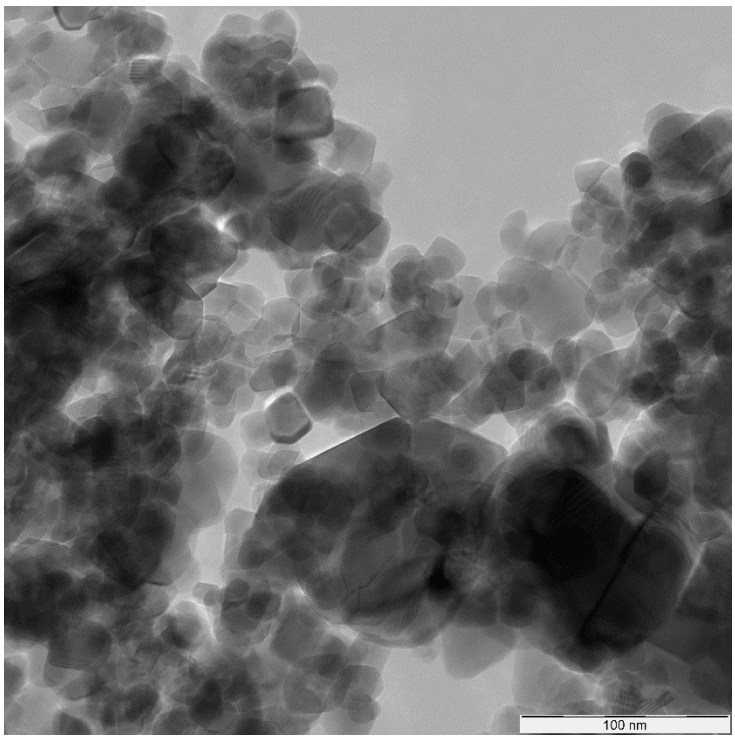

Figure 4-12 TEM micrographs of 1.0Fe400_1

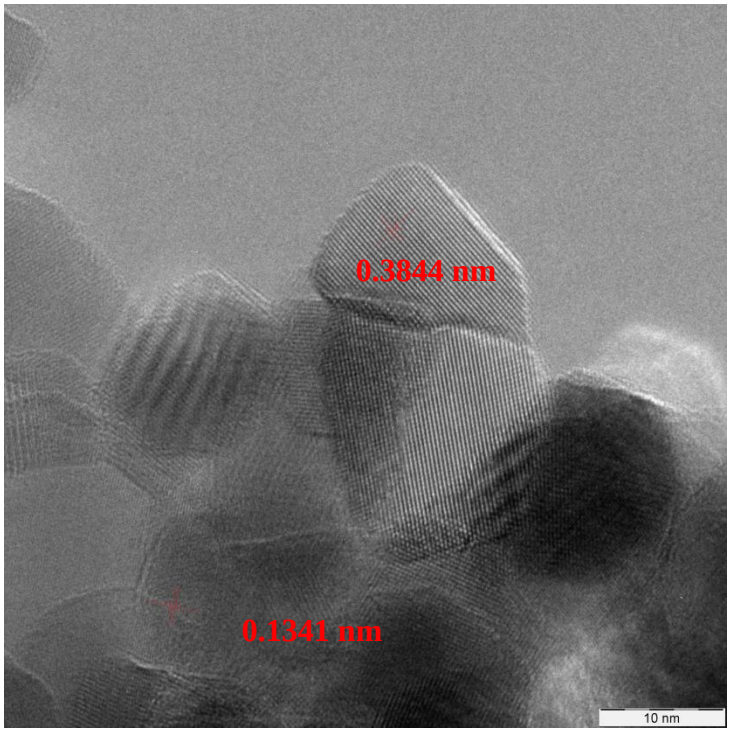

Figure 4-13 Fringes of the 1.0Fe400_1

4.1.6 Brunauer-Emmette-Teller (Surface Area & Porosity)

Table 4-7 BET surface area, pore volume, and pore size distribution of Fe-doped TiO_2

	Surface Area(m^2/g)	Pore Volume(cm^3/g)	Pore Size (Å)
0.2Fe400_1	46.5484	0.000054	245.950
0.2Fe500_1	42.1150	0.322183	300.8281
1.0Fe400_1	46.9689	0.358957	299.9290

Table 4-7 showed that the increasing amount of Fe loading could enhanced the surface area which is producing more pores inside the composites (Farhangi, Ayissi, & Charpentier, 2014). By comparing 0.2Fe400_1 and 0.2Fe500_1, there is a decrease of surface area as the calcination temperature increase. This is due to the agglomeration of TiO_2 nanoparticles and the collapse of the porous structure.

4.1.7 Diffuse Reflectance UV-visible spectra (DRUV-Vis)

The absorbance and diffuse reflectance is analyzed at the range of 200nm to 800nm. From *Figure 4-14*, P25 showed that there it is not photoactivate in visible region (400-800nm) (Feng, Yu, & Zhang, 2013). In order to harvest the energy at visible region, the absorbance of TiO_2 needed to be shifted. Fe doping on TiO_2 could significantly affects the absorption properties. The band gap energies of photocatalysts and Degussa P25 (Figure 4-14, Table 4-8) are determined by diffuse reflectance and calculated by the formula below: $E = hv$ where $v = \frac{c}{\lambda}$ (Farhangi, Ayissi, & Charpentier, 2014). It is observed that with the increase of Fe loading and temperature, the band gap energy is reduced.

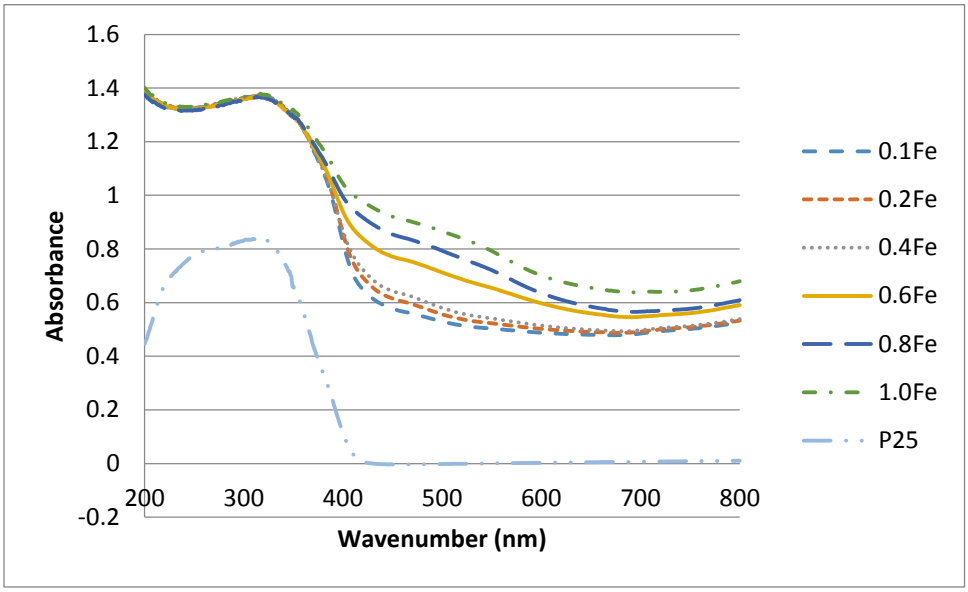

Figure 4-14 The DR-UV-Vis spectra of different loading of Fe on TiO_2

Table 4-8 The band gap energy of different loading of Fe and TiO_2

Samples	Band Gap Energy (eV)
0.1Fe	2.52
0.2Fe	2.48
0.4Fe	2.45
0.6Fe	2.36
0.8Fe	2.28
1.0Fe	2.16
P25	3.02

0.2Fe400_1	2.42
0.2Fe500_1	2.37
1.0Fe400_1	2.02

Conclusion

As a conclusion, this project is important as it could find alternative ways to desulfurize diesel oil by using TiO_2 followed by metal ion in visible light condition. It might encounter or improving the current problem by improving the characteristics of TiO_2. Photocatalysis by functioning with a metal species is believed to be more effective on the reaction performance.

A total of 6 batches of Fe/TiO_2 were prepared by wet-impregnation method. These catalysts were prepared in 0.1wt%, 0.2wt%, 0.4wt%, 0.6wt%, 0.8 wt% and 1.0wt% of Fe loading with calcination temperature of 350^oC, 400^oC and 450^oC. From the TGA results, it shows that starting from 350^oC is the best calcination temperature. After calcination, the nitrate functional group is totally removed. With the high concentration of Fe loading on TiO_2, it would reduce the particle size and so it reduces the band gap of photocatalyst which could increase the photonic efficiency.

Recommendation

In order to enhance the photo-oxidation process, some of the improvements need to be expends:

1. Preparation of Fe/TiO_2 by different method such as sol-gel method and more which give smaller particle size and could perform better.
2. Synthesis TiO_2 instead of using the commercial TiO_2 (Degussa P25).
3. To conduct desulfurization process.

References

Background information - What is transmission electron microscopy. (2013, March 5). Retrieved from MyScope training for advanced research: http://www.ammrf.org.au/myscope/tem/background/

Abbott, A. P., Harris, R. C., Ryder, K. S., D'Agostino, C., Gladden, L. F., & Mantle, M. D. (2011). Glycerol eutectics as sustainable solvent systems. *Royal Society of Chemistry*, *13*, 82-90.

Al-Rasheed, R. A. (2005). Wastewater treatment by Heterogeneous Photocatalyst: An Overview. In: Prsentend at the 4th SWCC acquired experience symposium. Jeddah.

Bin Li, a. M., Shi, Y., Ye, D., Wu, J., & Zhao, D. (2013). A Facile Strategy for the Preparation of Well-Dispersed Bimetal Oxide CuFe2O4 Nanoparticles Supported on Mesoporous Silica. Retrieved from http://www.rsc.org/suppdata/ta/c3/c3ta10506g/c3ta10506g.pdf

Farhangi, N., Ayissi, S., & Charpentier, P. A. (2014, March). Fe doped TiO2–graphene nanostructures:synthesis, DFT modeling and photocatalysis. *Nanotechnology*.

Fassier, M., Peyratout, C., Smith, D., Ducroquetz, C., & Voland, T. (2010, October). Photocatalytic activity of titanium dioxide coatings: Influence of the firing temperature of the chemical gel. *Journal of the European Ceramic Society, 30*(13), 2757–2762.

Feng, H., Yu, L. E., & Zhang, M.-H. (2013). Ultrasonic synthesis and photocatalytic performance of metal-ions doped TiO2 catalysts under solar light irradiation. *Materials Research Bulletin, 48*, 672–681.

Kulkarni, P. S., & Afonso, C. A. (2010). Deep desulfurization of diesel fuel using ionic liquids: current status and future challenges. *Green Chemistry*, *12*(7), 1139.

Kundu, T. K., & Chakravorty, D. (1999). Synthesis and Characterization of Nanocomposite Films with a Titania Glass Matrix by the Sol±gel Route. *Appl. Organometal. Chem.*, *13*, 353–360.

Li, D., Haneda, H., Hishita, S., & Ohashi, N. (2005). Visible-light driven Nitrogen doped TiO2 Photocatalysis: Effect og Nitrogen Precursors on their Photocatalysts for Decomposition of Gas-phase Organice Polluntants. *Maerial Science and Engineering B, 117*, 67-75.

Li, W., & Zeng, T. (2011, June 15). Preparation of TiO2 anatase nanocrystals by TiCl4 hydrolysis with additive H2SO4. *PLoS One, 6*(6).

Linacero, R., Aguado-Serrano, J., & Rojas-Cervantes, M. L. (2006). Preparation of. *Journal of Materials, 41*, 2457-2464.

Matei, E., Predescu, A. M., Predescu, A., Vasile, E., & Predescu, C. (2011, March). Investigations on nano-iron oxides properties used for different industrial applications. *OPTOELECTRONICS AND ADVANCED MATERIALS – RAPID COMMUNICATIONS, 5*(3), 296 - 301.

Moan, J. (2001). *Visible Light and UV Radiation.* Retrieved from http://www.uio.no/studier/emner/matnat/fys/FYS3610/h04/undervisningsmateriale/Moan 7.pdf

Mochizuki, Y., & Sugawara, K. (2008, July 23). Removal of Organic Sulfur from Hydrocarbon Resources Using Ionic Liquids. *Energy Fuels, 22*, 3303.

NACS. (2014). Retrieved August 12, 2014, from NACS: NACS. http://www.nacsonline.com/YourBusiness/FuelsReports/GasPrices_2014/Fuels/Pages/Diesel-Fuel-A-New-Growth-Market.aspx

Niu, H., Qing, Y., & Kaibin, T. (2006). A New Route to Copper Nitrate Hydroxide. *Materials Science and Engineering B, 135*, 172-175.

Porkodi, K., & Arokiamary, S. D. (n.d.). Synthesis and Spectroscopic Characterization of Nanostructured anatase Titania: A Photocatalyst. *Materials, 58*, 495-503.

Sarda, K. K., Bhandari, A., Pant, K. K., & Jain, S. (2012, October). Deep desulfurization of diesel fuel by selective adsorption over Ni/Al2O3 and i/ZSM-5 extrudates. *Fuel, 93*(1), 86–91.

Singh, P. (2009, June 8). *My Say: Malaysia slow on clean fuel initiatives.* Retrieved from http://www.theedgemalaysia.com/commentary/17877-my-say-malaysia-slow-on-clean-fuel-initiatives.html

Swapp, S. (2013, December 14). *Scanning Electron Microscopy (SEM).* Retrieved from Geochemical Instrumentation and Analysis: http://serc.carleton.edu/research_education/geochemsheets/techniques/SEM.html

Wang, J. L., Zhao, D. S., Zhou, E. P., & Dong, Z. (2007, June). Desulfurization of Gasoline by Extraction with N-alkylpyridinium-Based Ionic Liquids. *Journal of Fuel Chemistry and Technology., 35*, 293-296.

Wang, L., Cai, H., Lia, S., & Mominou, N. (2013, March). *Ultra-deep removal of thiophene compounds in diesel oil over catalyst TiO2/Ni-ZSM-5 assisted by ultraviolet irradiating*. Retrieved from Fuel: http://www.sciencedirect.com/science/article/pii/S001623611200782X

Yan, X., He, J., Evans, D. G., Zhu, Y., & Duan, X. (2004). Preparation, Characterization and Photocatalytic Activity of TiO2 Formed from a Mesoporous Precursor. *Journal of Porous Materials, 11*, 131-139.

Zhang, B., Jiang, Z., Li, J., Zhang, Y., Lina, F., Liu, Y., et al. (2012, March). Catalytic oxidation of thiophene and its derivatives via dual activation for ultra-deep desulfurization of fuels. *Journal of Catalysis*, 5-12.

Zhang, Z., Wang, C.-C., Zakaria, R., & Ying, J. Y. (1998, July). Role of Particle Size in Nanocrystalline TiO2-Based Photocatalysts. *J. Phys. Chem. B, 102*, 10871-10878.

Zhao, D. S., Wang, J. L., & Zhou, E. P. (2007). Oxidative desulfurization of diesel fuel using a Brønsted acid room temperature ionic liquid in the presence of H2O2. *Green Chemistry, 11*, 1219.

Appendices

Appendix A: Amount of Fe doping

Chemicals	Molar Mass, g/mol
Iron(III) Nitrate, $Fe(NO_3)_3 \cdot 9H_2O$	403.86
Iron, Fe	55.85
Titanium Dioxide, TiO_2	79.87

Figure A 1 Molar mass of the chemicals

Example calculation for 1wt% Fe doping

100g of catalyst required 1g of Fe metal.

By using gravimetric calculation,

$1\ mol\ of\ Fe(NO_3)_3\ .9H_2O \rightarrow 55.85g\ Fe$

$x\ mol\ of\ Fe(NO_3)_3\ .9H_2O \rightarrow 0.1g\ Fe$

$$\therefore x = \frac{0.1g\ Fe}{55.85g\ Fe} \times 1mol\ of\ Fe(NO_3)_3\ .9H_2O = 1.79 \times 10^{-3}mol$$

$1\ mol\ of\ Fe(NO_3)_3\ .9H_2O \rightarrow 403.86g\ of\ Fe(NO_3)_3\ .9H_2O$

$1.79 \times 10^{-3}\ mol\ of\ Fe(NO_3)_3\ .9H_2O\ \rightarrow y\ g\ of\ Fe(NO_3)_3\ .9H_2O$

$$\therefore y = \frac{1.79 \times 10^{-3}\ mol\ of\ Fe(NO_3)_3\ .9H_2O}{1\ mol\ of\ Fe(NO_3)_3\ .9H_2O} \times 403.86g\ of\ Fe(NO_3)_3\ .9H_2$$

$$= 0.7223g\ of\ Fe(NO_3)_3\ .9H_2O$$

$$Mass\ of\ TiO_2 = 10g - 0.7223g = 9.2777g$$

Similar calculations for 0.2 wt%, 0.4 wt%, 0.6 wt%, 0.8 wt% and 1.0 wt% Fe doping of TiO_2.

Metal loading, wt%	0.1	0.2	0.4	0.6	0.8	1.0
Mass of $Fe(NO_3)_3 \cdot 9H_2O$, g	0.7231	1.4462	2.8925	4.3387	5.7849	7.2312
Mass of TiO_2, g	9.2769	8.5538	7.1075	5.6613	4.2151	2.7688

Figure A 2 Summary of Fe doping on TiO_2

Appendix B: Preparation of Model Diesel

Dibenzothiophene, $C_{12}H_8S$ = 184.26 g/mol

Sulfur = 32 g/mol

Example calculation for 10ppm of sulfur

$1000ml\ of\ solution \rightarrow 10\ mg\ of\ sulfur$

$100ml\ of\ solution \rightarrow 1mg\ of\ sulfur\ (0.001\ g)$

$184.26\ g\ of\ DBT \rightarrow\ 32\ g\ of\ Sulfur$

$x\ g\ of\ DBT \rightarrow\ 0.001\ g\ of\ Sulfur$

$$x = \frac{0.001\ g\ of\ Sulfur}{32\ g\ of\ Sulfur} \times 184.26\ g\ of\ DBT = 0.0058g$$

In 100 mL of solution, 0.0058g of DBT is required to obtain 10ppm sulfur species in the model oil. Similar calculation for 20 ppm, 40 ppm, 60 ppm, 80 ppm, 100 ppm, 200 ppm, 300ppm and 400 ppm.

Amount of Sulfur, ppm	Amount of DBT ,g
10	0.0058
20	0.0115
40	0.0230
60	0.0345
80	0.0461
100	0.0576
200	0.1152
300	0.1727
400	0.2303

Figure A 3 Amount of DBT used for GC calibration

Appendix C: FTIR Spectra

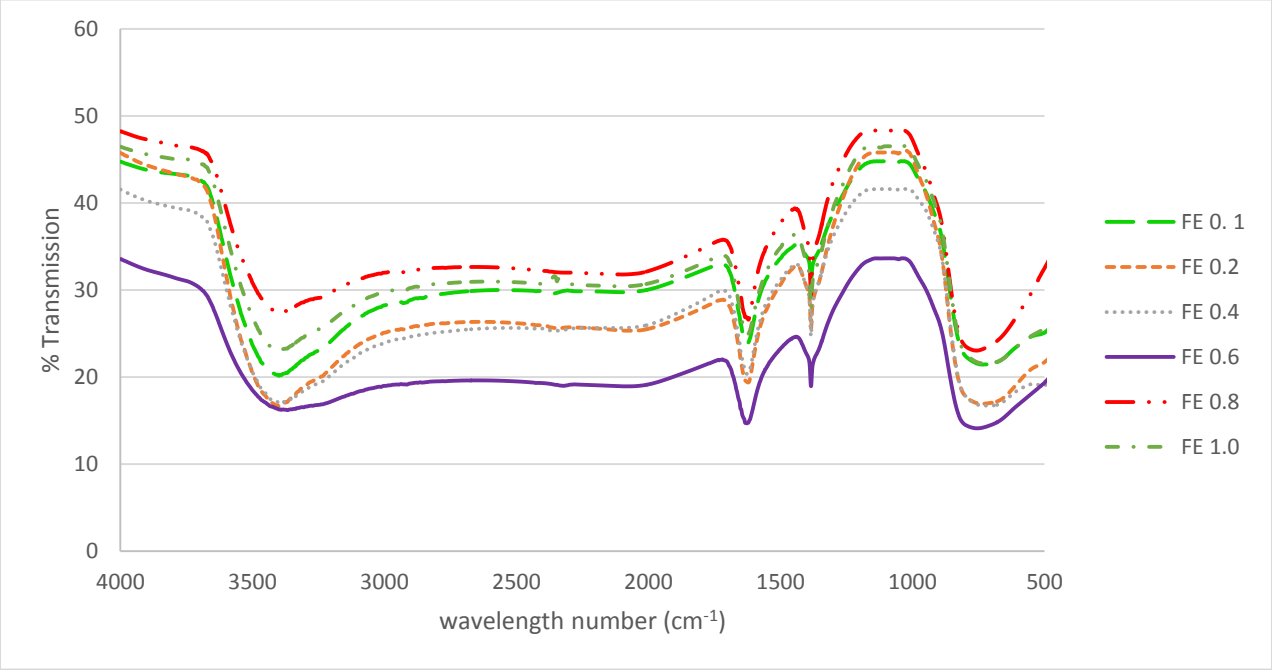

Figure C 1 FTIR spectra of uncalcined Fe/TiO_2 with different loading of Fe

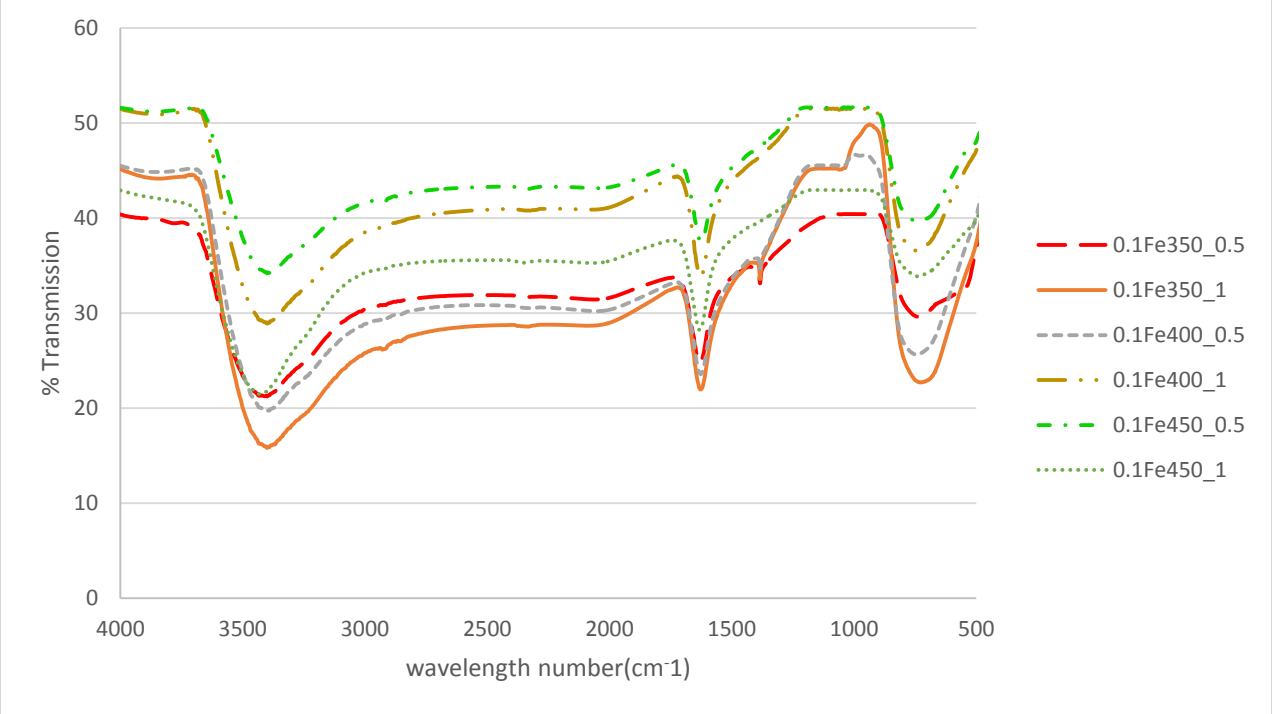

Figure C 2 FTIR spectra for 0.1wt% of Fe/TiO_2 at different calcination temperature and duration

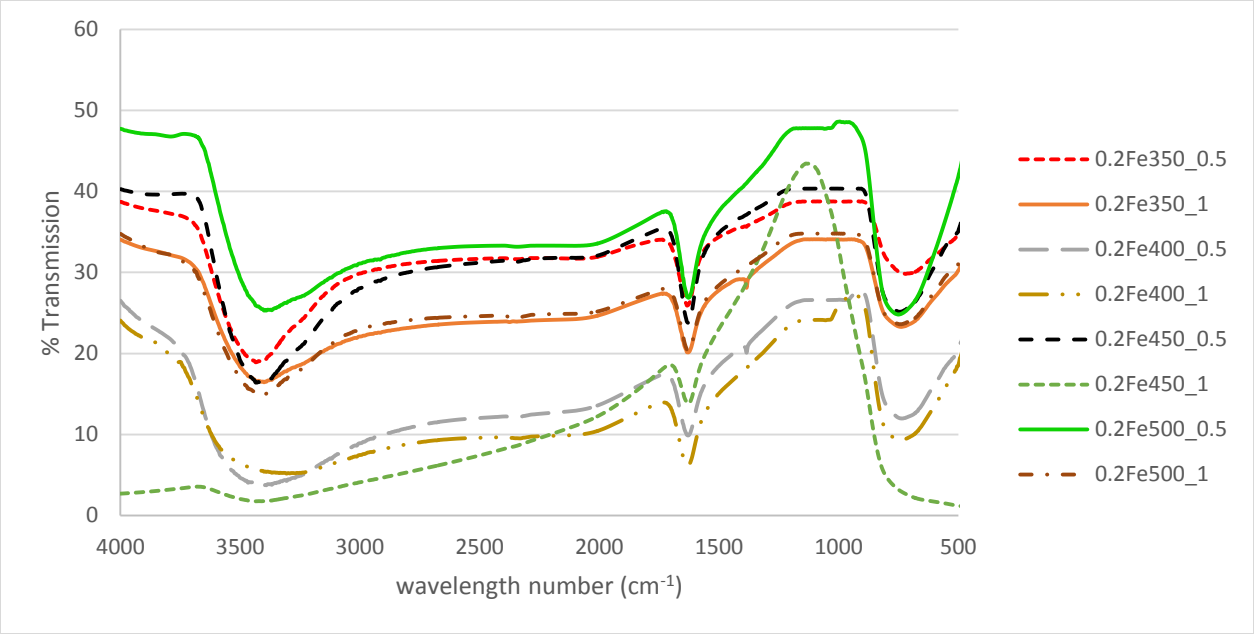

Figure C 3 FTIR spectra for 0.2wt% of Fe/TiO_2 at different calcination temperature and duration

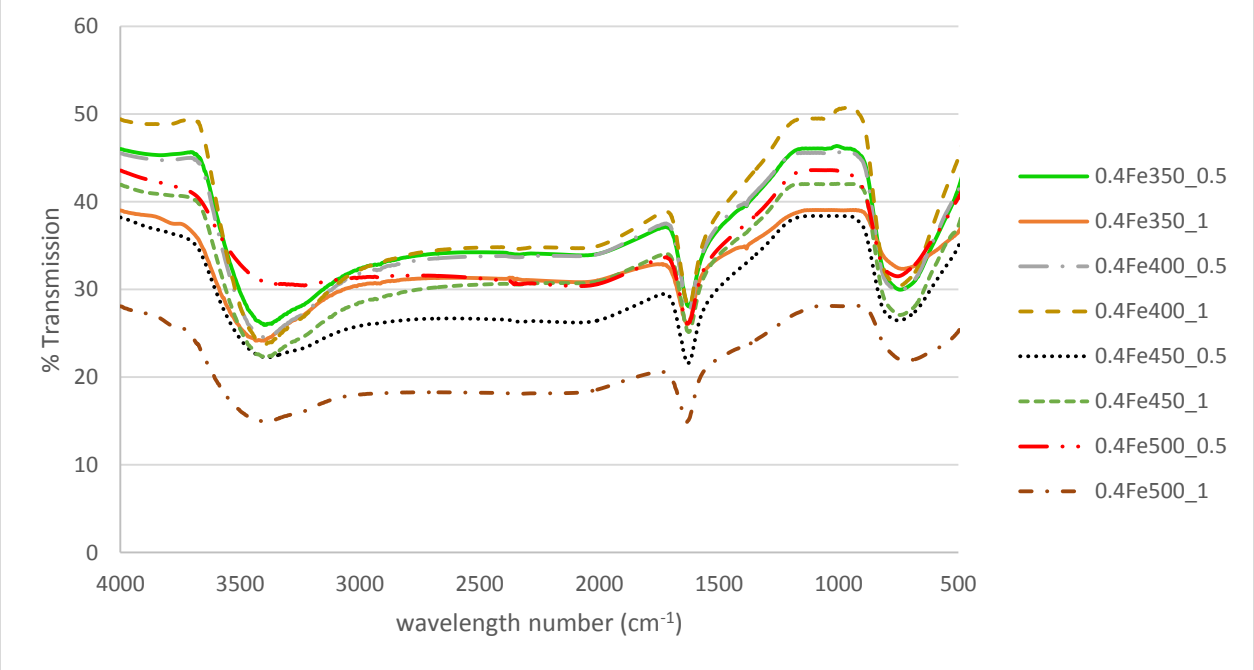

Figure C 4 FTIR spectra for 0.4wt% of Fe/TiO_2 at different calcination temperature and duration

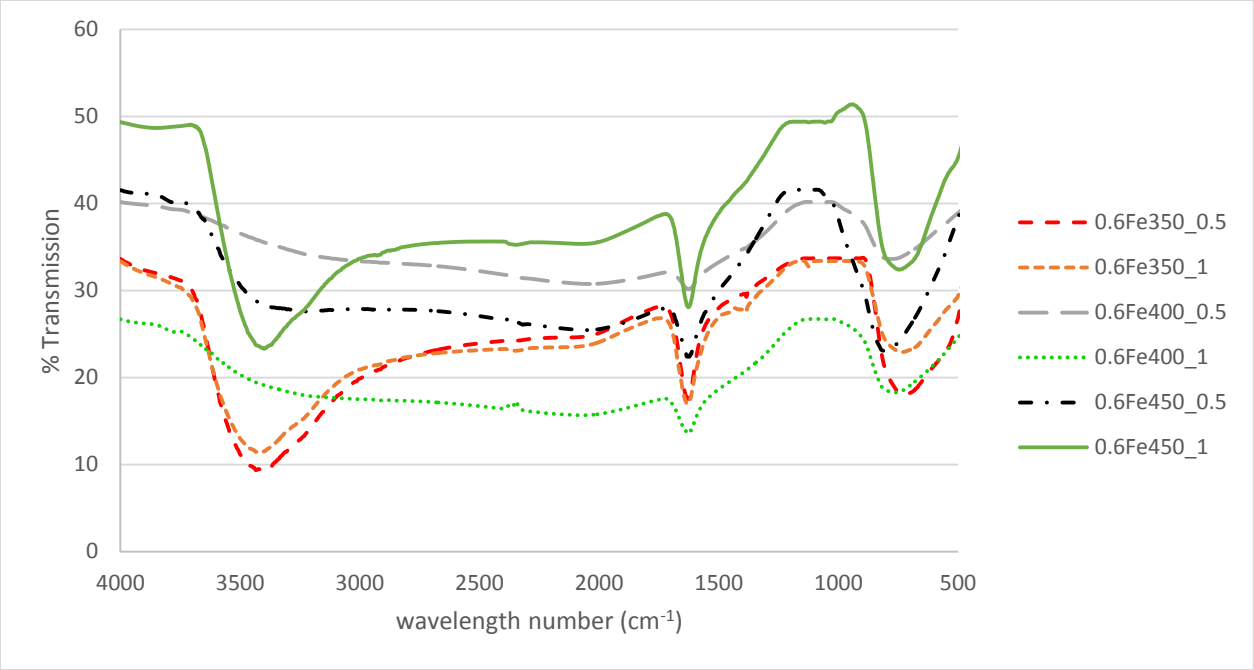

Figure C 5 FTIR spectra for 0.6wt% of Fe/TiO_2 at different calcination temperature and duration

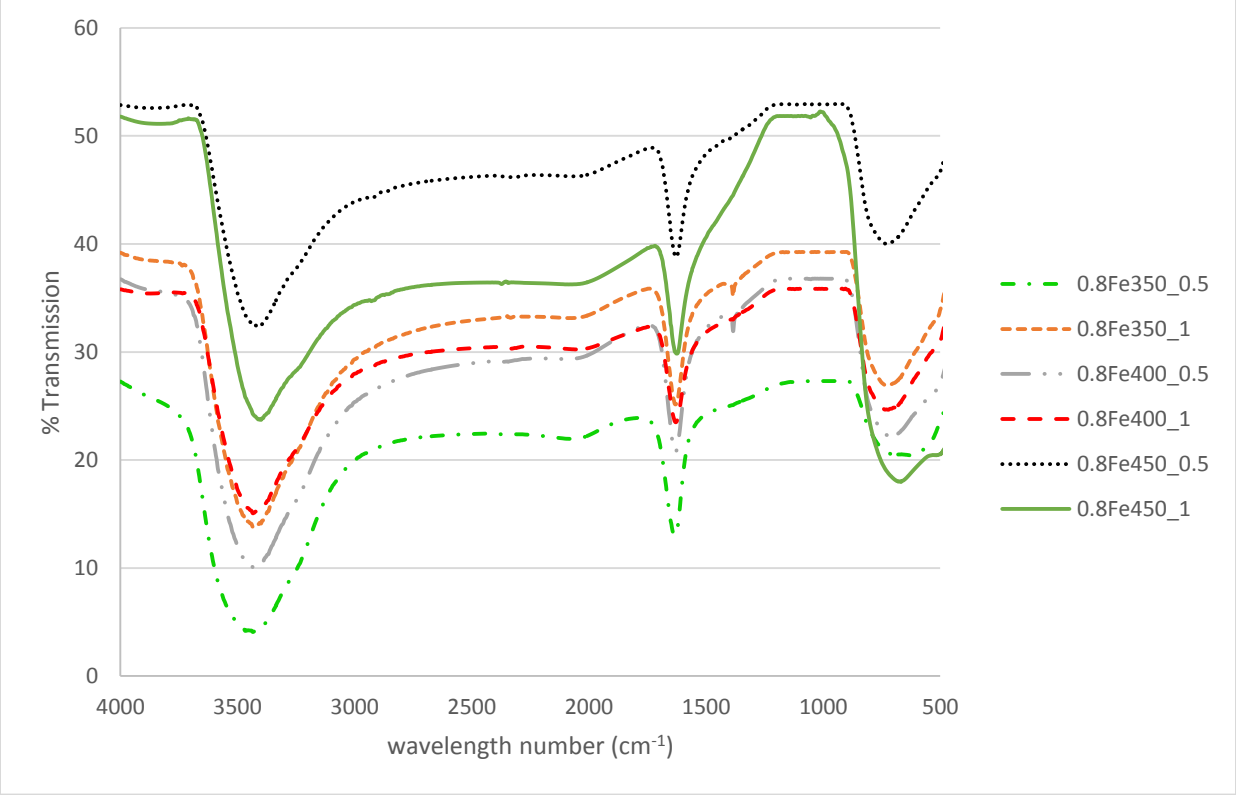

Figure C 6 FTIR spectra for 0.8wt% of Fe/TiO_2 at different calcination temperature and duration

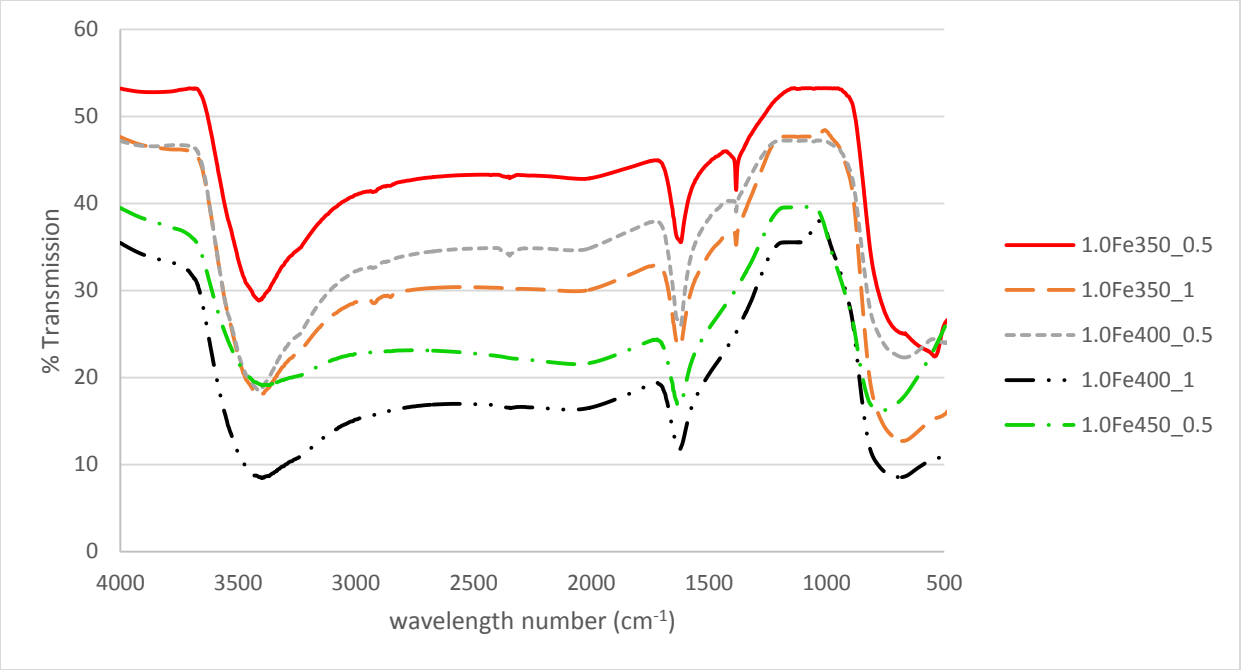

Figure C 7 FTIR spectra for 1.0wt% of Fe/TiO_2 at different calcination temperature and duration